ARTICLES
https://doi.org/10.1038/s41561-019-0524-2
nature geoscience

Global picophytoplankton niche partitioning predicts overall positive response to ocean warming

Pedro Flombaum[1,2,3], Wei-Lei Wang[1], Francois W. Primeau[1] and Adam C. Martiny[1,4]*

Ocean phytoplankton biomass is predicted to decline in Earth system models, due in large part to an expansion of nutrient-deplete ocean regions. However, the representation of ecosystems in these models is simplified and based on only a few functional types. As a result, they fail to capture the high diversity known to exist within and across phytoplankton communities. Here we present an assessment of the global biogeography of the very abundant but little studied picoeukaryotic phytoplankton by analysing a global abundance dataset with a neural-network-derived quantitative niche model. Combining this niche model with previous assessments of the distribution of *Prochlorococcus* and *Synechococcus*, we find that different cell sizes among picophytoplankton lineages are clearly partitioned into latitudinal niches. In addition, picophytoplankton biomass increases along a temperature gradient in low-latitude regions. We infer that future warmer ocean conditions can lead to elevated phytoplankton biomass in regions that are already dominated by picophytoplankton. Finally, we demonstrate that elevated upper-ocean nutrient recycling and lower nutrient requirements of phytoplankton have the potential to support increasing low-latitude phytoplankton biomass with future warming.

Earth system models are important for predicting the impact of climate change on marine ecosystems. Such models have been designed primarily for mechanistically describing carbon and nutrient fluxes. However, models are increasingly called upon for predicting ecosystem behaviour, including changes in the standing stock of ocean phytoplankton[1,2]. There is general agreement of a future decline in phytoplankton biomass due largely to an expansion of oligotrophic regions and the replacement of larger phytoplankton with picophytoplankton[3,4]. However, phytoplankton biomass predictions are uncertain for at least two reasons. First, model-predicted phytoplankton biomass is only cursorily calibrated by remotely sensed chlorophyll concentrations. However, the chl/C ratio can vary depending on phytoplankton diversity and physiology[5], leading to high uncertainty in chlorophyll-based estimates of phytoplankton biomass[6]. Second, Earth system models use a simplified ecosystem and few phytoplankton functional types[7]. This approach requires identifying and assigning a single set of growth parameters for a broad group of phytoplanton[8] and fails to capture the high diversity present in phytoplankton communities[9]. Thus, the unknown role of phytoplankton diversity could impede our ability to reliably predict how biomass will respond to growing environmental changes[6,8,10,11].

High intraspecific diversity can enable a lineage to grow across broad environmental conditions, leading to a wider fundamental niche than predicted from individual genotypes (Extended Data Fig. 1)[12]. Thus, an alternative to Earth system models for predicting future changes to phytoplankton abundances is to establish realized niche models by statistically quantifying abundances along ocean environmental gradients[13,14]. This approach is based on a simple tenet that the best estimate for future abundances is to find regions in the contemporary ocean with analogous environmental conditions (Extended Data Fig. 1). A niche model lacks a mechanistic basis for the distribution of phytoplankton but implicitly 'embraces' the within-lineage diversity, interactions between environmental factors and poorly understood biotic effects of other organisms.

We previously applied a niche model approach to project how *Prochlorococcus* and *Synechococcus* will respond to future ocean conditions[10]. However, we are missing a key phytoplankton group with a substantial but unconstrained biomass: the globally distributed and highly diverse picoeukaryotic phytoplankton assemblage[15–17]. Combined, these three groups constitute the picophytoplankton fraction and nearly all photosynthetic biomass in tropical and subtropical oligotrophic waters[18,19]. Thus, future climate projections of total phytoplankton biomass in low latitude ocean regions must include picoeukaryotic phytoplankton.

Here, we combined a global dataset and machine learning and asked what is the abundance and quantitative distribution of picoeukaryotic phytoplankton? We next combined this niche model with ones for *Prochlorococcus* and *Synechococcus* and asked how environmental factors influence the abundance and niche partitioning among these lineages and, finally, how total picophytoplankton biomass will respond to future projected climate changes.

Global biogeography of picoeukaryotic phytoplankton

We estimated an annual globally integrated abundance of picoeukaryotic phytoplankton of 1.6×10^{26} ($\pm1.8\times10^{25}$) cells. Using a neural-network-derived quantitative niche model trained on a geographically diverse dataset (Extended Data Fig. 2 and Supplementary Table 1), we captured a substantial part of the global variability (Extended Data Fig. 3, $R^2=0.46\pm0.01$). Regions of elevated concentrations ($>10^4$ cells ml^{-1}) included an area above 45° N in the North Atlantic Ocean, around the North Pacific Current, and a band near the southern subtropical convergence zone (Fig. 1). Picoeukaryotic phytoplankton were also projected in high abundances near upwelling zones, including the eastern equatorial Pacific Ocean, the California Current and the Benguela upwelling zone. Lower abundances were predicted for the oligotrophic gyres and polar regions. We also observed seasonal changes with a globally integrated abundance minimum of 1.4×10^{26} ($\pm1.1\times10^{25}$) cells and a maximum

[1]Department of Earth System Science, University of California, Irvine, CA, USA. [2]Centro de Investigaciones del Mar y la Atmósfera, CONICET, Buenos Aires, Argentina. [3]Universidad de Buenos Aires, Facultad de Ciencias Exactas y Naturales, Departamento de Ecología, Genética y Evolución, Buenos Aires, Argentina. [4]Department of Ecology and Evolutionary Biology, University of California, Irvine, CA, USA. *e-mail: amartiny@uci.edu

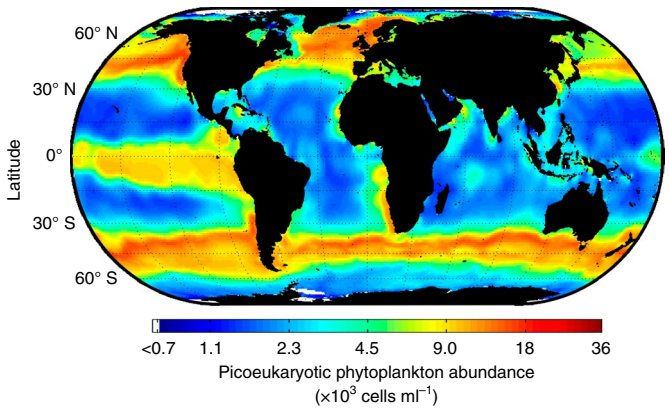

Fig. 1 | Global distribution picoeukaryotic phytoplankton abundance. Projected picoeukaryotic phytoplankton mean annual cell abundance at the sea surface as estimated by our niche model.

of 1.9×10^{26} ($\pm6.8\times10^{24}$) cells in June and September, respectively (Extended Data Fig. 4).

We quantified the niche for picoeukaryotic phytoplankton along light (photosynthetically active radiation (PAR)), temperature and nitrate gradients (Fig. 2). As expected for photosynthetic organisms, the abundance was 14 times higher in the surface compared with the deep euphotic zone light levels (Fig. 2a). In addition to light, there was a strong but nonlinear relationship between temperature and cell density (Fig. 2b). The abundance was lowest (1.8×10^{3} cells ml^{-1}) at 0 °C but increased to a maximum abundance (2.4×10^{4} cells ml^{-1}) at 8.5 °C. Beyond the maximum, the abundance declined and reached a local minimum at ~21 °C. Above this temperature, we saw an increase in cell numbers from 4×10^{3} to 12×10^{3} cells ml^{-1}, leading to intermediate concentrations in tropical waters. We also detected a nonlinear correlation between nitrate and abundance (Fig. 2c). Low nitrate concentrations had little effect, but abundance peaked at 1.6 µM of nitrate associated with a shift from 4×10^{3} to 1×10^{4} cells ml^{-1}. Above 1.6 µM, nitrate had a negative correlation to cell abundance, reaching a minimum of 2×10^{3} cells ml^{-1} at high nitrate concentrations. This hump-shaped distribution may be influenced by competition with *Prochlorococcus* and *Synechococcus* at the low end and larger phytoplankton at the high end of the nutrient gradient. The temperature or nitrate dependence of the predicted abundance did not change along gradients of the other variables, suggesting limited interaction terms for these factors. However, the effect of PAR was less pronounced at lower temperatures (Extended Data Fig. 5). In summary, picoeukaryotic phytoplankton displayed a clear global biogeography correlated with light, temperature and nutrient availability.

Niche portioning of picophytoplankton

We observed clear niche partitioning along gradients of light and temperature among *Prochlorococcus*, *Synechococcus* and picoeukaryotic phytoplankton (Fig. 3). The relative abundances of all lineages were generally positively influenced by increasing light levels (Fig. 3a). However, *Prochlorococcus* had a relative advantage at low light, and *Synechococcus* had a relative advantage at high light levels. Picoeukaryotic phytoplankton displayed an intermediate response. Small eukaryotic phytoplankton such as *Ostreococcus* strains show some light inhibition at elevated light levels (>1.6 E m^{-2} d^{-1}) but can still sustain intermediate growth rates[20,21]. By contrast, individual *Prochlorococcus* strains can grow at very low light levels but can be photoinhibited near the surface[22]. Further, some *Synechococcus* strains show little light inhibition even at extremely high light levels but cannot sustain growth at low intensities[22]. Thus, the distribution along a light gradient is consistent with physiological studies of the three groups. Our models also revealed niche partitioning along a temperature gradient that corresponded with cell size (Fig. 3b). The abundance of the largest-sized group, picoeukaryotic phytoplankton, peaked at 8.5 °C. The intermediate-sized *Synechococcus* peaked at 10 °C, whereas *Prochlorococcus*, as the smallest, was most common at high temperature. The growth rate in all three lineages generally responds positively to temperatures in this range, which should lead to an overall positive relationship between abundance and temperature[22,23]. However, the decline in

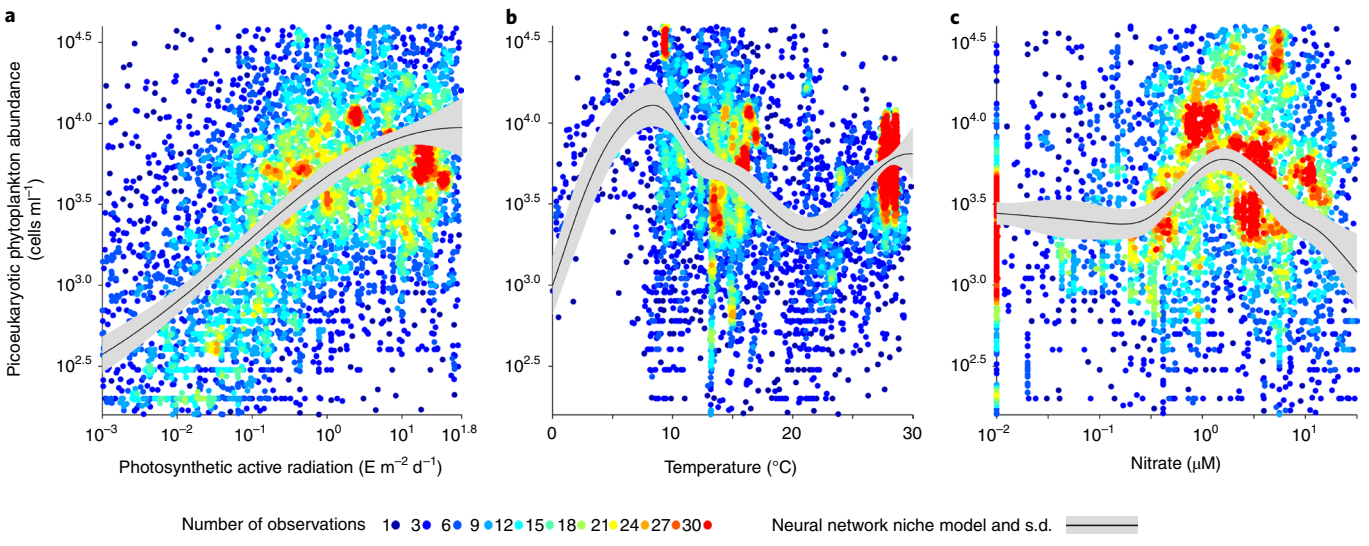

Fig. 2 | Picoeukaryotic phytoplankton observations and niche model predictions as a function of environmental variation. The line and shaded area represent the quantitative niche model output mean and s.d. based on 100 trained neural networks. **a**–**c**, The niche model represents cell abundance at constant temperature and nitrate (15 °C and 3.2 µM) (**a**), PAR and nitrate (3.2 E m^{-2} d^{-1} and 3.2 µM) (**b**) and PAR and temperature (3.2 E m^{-2} d^{-1} and 15 °C) (**c**). Symbol colour represents number of overlapping observations in intervals of PAR $10^{0\pm1.2}$ E m^{-2} d^{-1}, temperature 15 ± 7.5 °C and nitrate $10^{0.5\pm1}$ µM. See Extended Data Fig. 5 for interactions between terms.

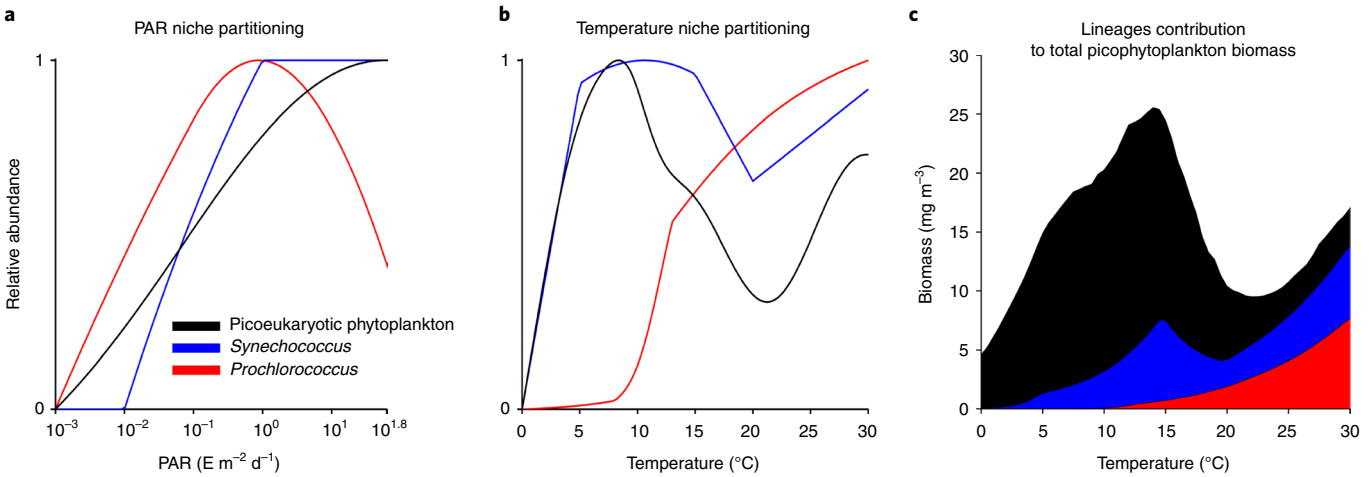

Fig. 3 | Niche partitioning among picoeukaryotic phytoplankton, *Synechococcus* and *Prochlorococcus*. a,**b**, Predicted cell abundance relative to the difference between minimum and maximum cells per millilitre as a function of PAR at constant temperature and nitrate concentration (**a**) and temperature at constant light and nitrate concentration (**b**). **c**, Contributions of picoeukaryotic phytoplankton, *Synechococcus* and *Prochlorococcus* to total picophytoplankton biomass as a function of temperature.

picoeukaryotic phytoplankton and *Synechococcus* at intermediate temperatures and the sharp decline in abundance of *Prochlorococcus* below 20 °C could result from competition with other phytoplankton linages. We then combined all models to predict changes in total picophytoplankton carbon biomass with temperature (Fig. 3c). Changes in picoeukaryotic phytoplankton controlled the cumulative biomass below ~20 °C, whereas especially changes in *Prochlorococcus* abundance were important above this threshold. Combined, total picophytoplankton biomass increased with temperature above ~20 °C.

Global current and future picophytoplankton biomass

We next quantified the total picophytoplankton carbon biomass in the global ocean as well as the contribution by each lineage. The combined mean annual picophytoplankton biomass was 0.55 ± 0.03 Pg of C in the global ocean and thus higher than most biogeochemical model estimations[7] but smaller than earlier projections[24]. Picoeukaryotic phytoplankton, *Synechococcus* and *Prochlorococcus* contributed 45%, 27% and 27% of total picophytoplankton carbon biomass, respectively. The niche partitioning of each lineage along a temperature gradient translated into regional differences in contribution to surface carbon biomass (Fig. 3c and Extended Data Fig. 6a–c). Picoeukaryotic phytoplankton dominated picophytoplankton biomass at high latitudes and upwelling regions (Extended Data Fig. 6a). At lower latitudes, Cyanobacteria were more common, with *Prochlorococcus* contributing slightly higher biomass proportions than *Synechococcus* (Extended Data Fig. 6b,c). The combined picophytoplankton biomass varied between ~5 mg m^{-3} of C in the oligotrophic gyres to ~25 mg m^{-3} of C in temperate regions with high picoeukaryotic phytoplankton abundances (Extended Data Fig. 6d).

We compared our biomass estimations with an Earth system model (GFDL ESM2) prediction for the current ocean. Picophytoplankton constituted 53% of global ocean surface phytoplankton biomass and were generally equal to (or slightly above) a global community ecosystem model estimate of total phytoplankton biomass in most regions between 60° N and 60° S (Extended Data Fig. 6e)[18]. As expected, picophytoplankton contributed less to overall biomass in polar regions and some upwelling zones, where larger phytoplankton lineages proliferate. Our biomass estimate was up to 50% higher than past model assessments in some regions, including warm parts of the oligotrophic gyres (for example, the Western Pacific Warm Pool). Thus, there was substantial discrepancy between our estimated picophytoplankton biomass levels and the GFDL ESM2 global model predictions.

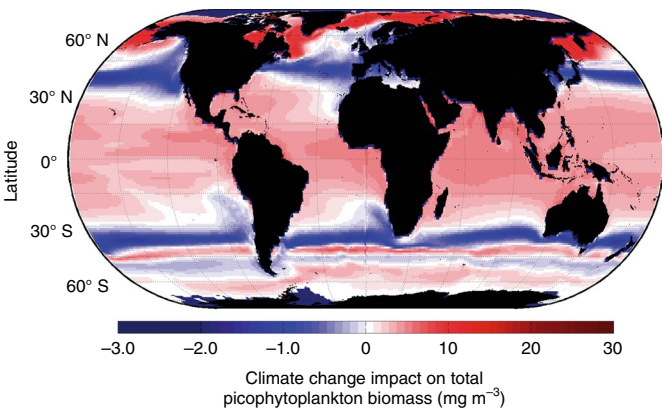

Fig. 4 | Projected impact of climate change on total picophytoplankton carbon biomass. Difference in surface total picophytoplankton carbon biomass estimated for the end of the twenty-first and twentieth centuries on the basis of temperature and nitrate concentration simulated under the RCP 8.5 and historic CMIP5 scenarios.

Finally, we combined niche models with estimates of future ocean conditions to predict how total picophytoplankton biomass could respond to climate change. Picophytoplankton biomass was sensitive to projected ocean environmental changes and showed a global increase of 0.05 ± 0.02 Pg of C under the high-emission representative concentration pathway (RCP) 8.5 scenario. Mean surface carbon biomass between 30° N and 30° S was 12 ± 2.4 and 15 ± 1.9 mg m^{-3} for the historic and RCP 8.5 scenarios, respectively (Fig. 4 and Extended Data Fig. 7). However, there were big geographical differences leading to regions with strong declines (primarily upwelling regions and a temperate band around 40°) or increases (for example, tropical Indian Ocean). The change in total picophytoplankton biomass was driven by parallel increases of *Synechococcus* and *Prochlorococcus* between 20 °C and 30 °C, whereas integrated picoeukaryotic phytoplankton biomass stayed flat (Fig. 3c). As total picophytoplankton constitutes nearly all biomass in oligotrophic regions[18,19], we can use the combined niche

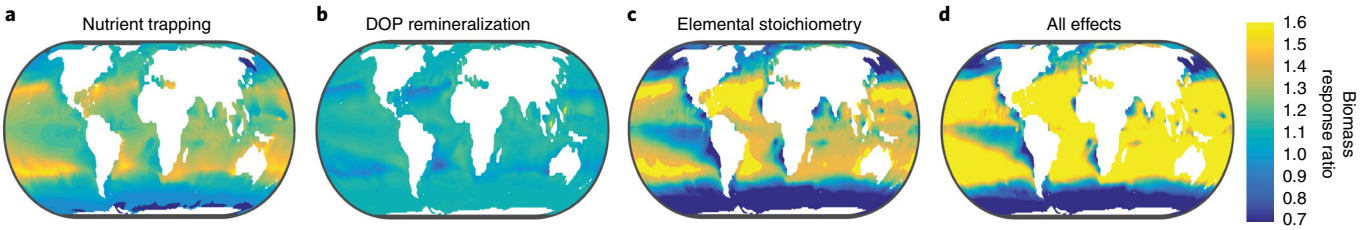

Fig. 5 | Evaluation of ecosystem regulation mechanisms on phytoplankton biomass. a–d, Impact of increased nutrient retention (**a**), DOP remineralization (**b**), elemental stoichiometry (**c**) and the combined effect (**d**) for the top 35 m of ocean biomass.

models as an independent estimate for how low-latitude total phytoplankton biomass will respond to environmental changes. Thus, our projection suggests elevated picophytoplankton and probably total phytoplankton biomass in most low-latitude regions in response to projected future climate changes.

Possible mechanisms controlling picophytoplankton biomass

Most conceptual and biogeochemical models suggest that biomass in low-latitude regions is negatively related to stratification and associated nutrient supply[3]. However, phytoplankton biomass is controlled by complex growth and decay processes resulting in previously unrecognized links between environmental change and biomass. First, small particles may be exported less efficiently and organic material is respired faster at high temperature[25]. As seen for particulate iron[26], the combined effect is a temperature-dependent upper-ocean nutrient retention supporting additional growth. This nutrient retention effect can be illustrated with a box model (Extended Data Fig. 8). Here, phytoplankton biomass in the surface ocean is augmented when biomass and nutrients are recycled near the surface. Second, the large stock of organically bound nutrients (for example, dissolved organic phosphorous (DOP)) may be more accessible at elevated temperatures[27]. Third, phytoplankton can sustain growth with stoichiometrically less nutrients in warm, oligotrophic environments[28,29]. Global biogeochemical simulation suggested that modest increases in upper ocean nutrient retention or frugal nutrient demand in phytoplankton could support elevated surface biomass across low-latitude regions independently of the vertical nutrient flux (Fig. 5 and Extended Data Fig. 9). By contrast, elevated remineralization of DOP led to only minor shifts in phytoplankton biomass. Temperature may also regulate the balance of phytoplankton growth and grazing, and there are indications that this ratio is positively related to temperature in oligotrophic ecosystems[30]. Thus, phytoplankton biomass is sensitive to complex temperature- and nutrient-driven ecosystem processes and not solely driven by the vertical nutrient flux.

This work presents a divergent future prediction for low-latitude phytoplankton biomass in a warming world. Earth system models predict a decline, whereas our machine-learning approach suggests a biomass increase. However, both approaches are associated with significant uncertainty. Biomass estimates in Earth system models are generally calibrated against chlorophyll despite known variations in chl/C and use a simplified ecosystem description. Niche models assume that phytoplankton biomass will share the same relationship to environmental parameters today and in the future and may lack important feedbacks. These uncertainties and the strongly divergent outcomes of the two approaches question the generally accepted prediction of future declines in low-latitude phytoplankton biomass. Before confident predictions can be made, the potential impacts such as efficient recycling of nutrients by diverse communities[8], phytoplankton with high C/nutrient biomass composition[31] and grazing[30] must be evaluated. Thus, our analyses indicate that a previously uncharacterized positive response in phytoplankton biomass to warming in low-latitude environments may be important to future ocean biology and ecosystem functioning.

Online content

Any methods, additional references, Nature Research reporting summaries, source data, extended data, supplementary information, acknowledgements, peer review information; details of author contributions and competing interests; and statements of data and code availability are available at https://doi.org/10.1038/s41561-019-0524-2.

Received: 4 June 2019; Accepted: 11 December 2019;
Published online: 27 January 2020

References

1. Hoegh-Guldberg, O. & Bruno, J. F. The impact of climate change on the world's marine ecosystems. *Science* **328**, 1523–1528 (2010).
2. Moore, J. K. et al. Sustained climate warming drives declining marine biological productivity. *Science* **359**, 1139–1143 (2018).
3. Bopp, L. et al. Multiple stressors of ocean ecosystems in the 21st century: projections with CMIP5 models. *Biogeosciences* **10**, 6225–6245 (2013).
4. Cabre, A., Marinov, I. & Leung, S. Consistent global responses of marine ecosystems to future climate change across the IPCC AR5 Earth system models. *Clim. Dyn.* **45**, 1253–1280 (2015).
5. Graff, J. R. et al. Photoacclimation of natural phytoplankton communities. *Mar. Ecol. Prog. Ser.* **542**, 51–62 (2016).
6. McQuatters-Gollop, A. et al. Is there a decline in marine phytoplankton? *Nature* **472**, E6–E7 (2011).
7. Quéré, C. Le et al. Ecosystem dynamics based on plankton functional types for global ocean biogeochemistry models. *Glob. Change Biol.* **11**, 2016–2040 (2005).
8. Lomas, M. W., Bonachela, J. A., Levin, S. A. & Martiny, A. C. Impact of ocean phytoplankton diversity on phosphate uptake. *Proc. Natl Acad. Sci. USA* **111**, 17540–17545 (2014).
9. Rusch, D. B. et al. The sorcerer II global ocean sampling expedition: northwest Atlantic through eastern tropical Pacific. *PLoS Biol.* **5**, e77 (2007).
10. Flombaum, P. et al. Present and future global distributions of the marine cyanobacteria *Prochlorococcus* and *Synechococcus*. *Proc. Natl Acad. Sci. USA* **110**, 9824–9829 (2013).
11. Irwin, A. J., Finkel, Z. V., Müller-Karger, F. E. & Troccoli Ghinaglia, L. Phytoplankton adapt to changing ocean environments. *Proc. Natl Acad. Sci. USA* **112**, 5762–5766 (2015).
12. Larkin, A. A. & Martiny, A. C. Microdiversity shapes the traits, niche space, and biogeography of microbial taxa. *Environ. Microbiol. Rep.* **9**, 55–70 (2017).
13. Irwin, A. J., Nelles, A. M. & Finkel, Z. V. Phytoplankton niches estimated from field data. *Limnol. Oceanogr.* **57**, 787–797 (2012).
14. Colwell, R. K. & Rangel, T. F. Hutchinson's duality: the once and future niche. *Proc. Natl Acad. Sci. USA* **106**, 19651–19658 (2009).
15. Moon-van der Staay, S. Y., De Wachter, R. & Vaulot, D. Oceanic 18S rDNA sequences from picoplankton reveal unsuspected eukaryotic diversity. *Nature* **409**, 607–610 (2001).
16. Li, W. K. W. From cytometry to macroecology: a quarter century quest in microbial oceanography. *Aquat. Microb. Ecol.* **57**, 239–251 (2009).
17. Morán, X. A. G., López-Urrutia, Á., Calvo-Díaz, A. & LI, W. K. W. Increasing importance of small phytoplankton in a warmer ocean. *Glob. Change Biol.* **16**, 1137–1144 (2010).
18. Bienfang, P. K., Szyper, J. P., Okamoto, M. Y. & Noda, E. K. Temporal and spatial variability of phytoplankton in a subtropical environment. *Limnol. Oceanogr.* **29**, 527–539 (1984).
19. Landry, M. R., Kirshtein, J. & Constantinou, J. Abundances and distributions of picoplankton populations in the central equatorial Pacific from 12° N to 12° S, 140° W. *Deep. Sea Res. Part 2 Top. Stud. Oceanogr.* **43**, 871–890 (1996).

20. Rodríguez, F. et al. Ecotype diversity in the marine picoeukaryote *Ostreococcus* (Chlorophyta, Prasinophyceae). *Environ. Microbiol.* **7**, 853–859 (2005).
21. Six, C. et al. Contrasting photoacclimation costs in ecotypes of the marine eukaryotic picoplankter. *Ostreococcus. Limnol. Oceanogr.* **53**, 255–265 (2008).
22. Moore, L. R., Goericke, R. & Chisholm, S. W. Comparative physiology of *Synechococcus* and *Prochlorococcus*: influence of light and temperature on growth, pigments, fluorescence and absorptive properties. *Mar. Ecol. Prog. Ser.* **116**, 259–275 (1995).
23. Kulk, G., De Vries, P., Van De Poll, W. H., Visser, R. J. W. & Buma, A. G. J. Temperature-dependent growth and photophysiology of prokaryotic and eukaryotic oceanic picophytoplankton. *Mar. Ecol. Prog. Ser.* **466**, 43–55 (2012).
24. Buitenhuis, E. T. et al. Picophytoplankton biomass distribution in the global ocean. *Earth Syst. Sci. Data* **4**, 37–46 (2012).
25. Rivkin, R. B. & Legendre, L. Biogenic carbon cycling in the upper ocean: effects of microbial respiration. *Science* **291**, 2398–2400 (2001).
26. Rafter, P. A., Sigman, D. M. & Mackey, K. R. M. Recycled iron fuels new production in the eastern equatorial Pacific Ocean. *Nat. Commun.* **8**, 1100 (2017).
27. White, A. E., Watkins-Brandt, K. S., Engle, M. A., Burkhardt, B. & Paytan, A. Characterization of the rate and temperature sensitivities of bacterial remineralization of dissolved organic phosphorus compounds by natural populations. *Front. Microbiol.* **3**, 276 (2012).
28. Martiny, A. C. et al. Strong latitudinal patterns in the elemental ratios of marine plankton and organic matter. *Nat. Geosci.* **6**, 279–283 (2013).
29. Martiny, A. C., Vrugt, J. A., Primeau, F. W. & Lomas, M. W. Regional variation in the particulate organic carbon to nitrogen ratio in the surface ocean. *Global Biogeochem. Cycles* **27**, 723–731 (2013).
30. Chen, B., Landry, M. R., Huang, B. & Liu, H. Does warming enhance the effect of microzooplankton grazing on marine phytoplankton in the ocean? *Limnol. Oceanogr.* **57**, 519–526 (2012).
31. Moreno, A. R. & Martiny, A. C. Ecological stoichiometry of ocean plankton. *Ann. Rev. Mar. Sci.* **10**, 43–69 (2018).

Methods

Dataset. All analyses were done using Matlab (Mathworks, MA). We obtained 13,771 picoeukaryotic phytoplankton observations from available public repositories and primary sources of a total of 39 cruises and time series covering major ocean regions and diverse environments (Extended Data Fig. 2 and Supplementary Table 1). Picoeukaryotic phytoplankton are defined as red fluorescent cells larger than *Prochlorococcus* and less than 2–3 µm in cell diameter. We only considered cell counts by flow cytometry. Samples covered a latitudinal range from 71.4° N to 66.1° S up to 400 m depth. Ancillary temperature and nitrate records were available for all but 2,334 and 6,530 observations, respectively, which we complemented with 1° monthly depth-dependent averages from the World Ocean Atlas (www.nodc.noaa.gov). To avoid analytical issues with detection limits, we imposed a minimum nitrate concentration of 0.01 µM. We calculated surface PAR (8 d averaged, 0.047° grid cell) using SeaWiFS and MODIS observations. Downward PAR was estimated using the attenuation coefficient K_{490} from SeaWiFS and MODIS (https://oceancolor.gsfc.nasa.gov/) and corrected for chlorophyll a (ref. [32]), and a minimum of 10^{-3} E m^{-2} d^{-1} was imposed.

Neural network analysis. To partition the nonlinear relationship and interactions between oceanographic factors and predict the overall distribution of picoeukaryotic phytoplankton, we trained a feed-forward back-propagation neural network with 10 nodes and up to 1,000 epochs[10]. We evaluated the inclusion of temperature, PAR ($\log_{10}$ transformed) and nitrate concentration ($\log_{10}$ transformed) and found that all three factors contributed to describing log-transformed abundances of picoeukaryotic phytoplankton. We used 50% of the observations for training (selected randomly) and the rest for validation. Optimization of the network was evaluated using Bayesian regularization. This process was repeated 100 times to estimate the variance in quantification. We then identified the contribution and interactions of environmental factors by sequentially varying each factor between the minimum and maximum observed value (100 steps). This was repeated across all 100 trained networks to assess any bias associated with the data selection, and the variation across the ensemble is the reported variance. Any bias regarding differences in cruises or in regional effects were not detected[10].

Biomass contribution. To estimate global cell abundance of picoeukaryotic phytoplankton, we used as input to our neural network models monthly average temperatures and nitrate from the World Ocean Atlas 2005 (1°×1° resolution) and PAR and K_{490} values derived from satellite data (SeaWiFS 0.083°×0.083°) and obtained predicted abundances for each set of conditions. We estimated annual globally integrated cell abundance by integrating monthly cell abundance from surface to 205 m deep (in layers of 10 m) and a 1°×1° resolution grid. We estimated the annual globally integrated cell abundance standard deviation using the 100 trained neural networks. For sea surface abundance, we used the first layer. As the neural network analysis was done in $\log_{10}$ space, we back-transformed cell abundances using a correction of 1.84 (the ratio of the mean in regular space against the lognormal mean). Cell abundances for *Prochlorococcus* and *Synechococcus* were estimated using existing quantitative niche models based on temperature and PAR[10]. We converted cell abundances to biomass using reported cellular carbon biomass content estimates for *Prochlorococcus* (50 fg $cell^{-1}$ of C), *Synechococcus* (175 fg $cell^{-1}$ of C) and picoeukaryotic phytoplankton (1,500 fg $cell^{-1}$ of C) (ref. [33]). Total picophytoplankton biomass was the sum of the three lineages. For total phytoplankton biomass, we reported values simulated by the GFDL ESM2 Earth system model[34].

Future predictions. To evaluate the effects of future climate change on picoeukaryotic phytoplankton abundance and biomass, we used as input to our neural network models year values of temperature and nitrate outputs from Earth system models under RCP 8.5 (equivalent to a radiative forcing of 8.5 W m^{-2} in 2100) and historical scenarios. Light fields were identical across simulations. We calculated the effect of climate change for each lineage and total picophytoplankton biomass as the difference between 2070–2099 and 1970–1999 for the RCP 8.5 and historical scenarios. We imposed a maximum sea surface temperature of 30 °C as model predictions of higher temperature are uncertain due to poorly constrained atmospheric convection feedbacks. The combination of temperature and nitrate in climate model projections for the end of the century were well represented in our observation dataset, and no extrapolation was necessary (Extended Data Fig. 10). We used an ensemble of eight Earth system models, CanESM2, CESM1 BGC, GFDL ESM2G, HadGEM2 ES, IPSL CM5A MR, MIROC ESM, MPI and NorESM1 ME[35], to estimate mean and standard deviation values for present and future projections. Standard deviation for climate change projection was estimated for the multimodel ensemble. It is important to note that we assume limited additional feedback between the predicted changes in phytoplankton abundances and nitrate concentration (that is, beyond what is already captured by the climate model).

Our predictions are based on some important assumptions. First, we assume perfect lineage niche conservatism[36] as the very large population size of lineages suggests selection among existing ecotypes rather than de novo mutations will likely be more common. Second, it is assumed that other abiotic as well as biotic interactions such as predation or competition with other lineages track the applied underlying environmental conditions. This may be a reasonable assumption to a first order as larger competing phytoplankton as well as grazers and viruses putatively are sensitive to the same underlying environmental ranges. Third, climate change may lead to environmental conditions not currently present in the ocean (for example, low pH), leading to changes in niches and future abundances not captured by our analysis.

Box model design for evaluating the impact of nutrient retention by phytoplankton in the euphotic layer. We developed a simple model to illustrate the effect of nutrient recycling and retention by phytoplankton in the euphotic layer (Extended Data Fig. 8). In particular, we wanted to demonstrate that the standing stock of phytoplankton is sensitive to the degree of nutrient recycling and retention. The model captures the major physical and biological processes controlling nutrient cycling in the upper ocean in terms of two prognostic variables: the living pool of nutrients in phytoplankton (P), and the dead pool of dissolved nutrients (N). Nutrients from the dead pool are taken up by phytoplankton in the upper ocean at a rate uPN and returned to the dead pool at a rate kP. The model includes a loss of nutrients by sinking particles at a rate sP, which is balanced by a net return flux $q(N_d - N)$, where N_d is the nutrient concentration in the deep ocean, which is assumed constant, and q is the water-mass exchange rate between the deep ocean and upper ocean. The differential equations governing these time (t) processes are:

$$\frac{dN}{dt} = qN_d + kP - qN - uNP \tag{1}$$

and

$$\frac{dP}{dt} = -(q + k + s)P + uNP \tag{2}$$

These equations can be re-expressed in non-dimensional form:

$$\begin{aligned} \tfrac{dn}{d\tau} &= 1 + rp - n - \gamma np \\ \tfrac{dp}{d\tau} &= -p - rp - \epsilon p + \gamma np \end{aligned} \tag{3}$$

in which we have rescaled the dependent and independent variables by N_d and q, respectively:

$$\begin{aligned} n &= \tfrac{N}{N_d} \\ p &= \tfrac{P}{N_d} \\ \tau &= qt \end{aligned} \tag{4}$$

and introduced the following dimensionless parameters:

$$\begin{aligned} \gamma &\equiv \tfrac{u}{q} N_d \\ r &\equiv \tfrac{k}{q} \\ \epsilon &\equiv \tfrac{s}{q} \end{aligned} \tag{5}$$

The steady-state solution, obtained by setting the time derivatives to zero, is given by:

$$\begin{aligned} n_{ss} &= \tfrac{1+r+\epsilon}{\gamma} \\ p_{ss} &= \tfrac{1}{1+\epsilon}\left(1 - \tfrac{1+r+\epsilon}{\gamma}\right) \end{aligned} \tag{6}$$

To simplify the preceding expression, we consider parameter values appropriate for low-latitude ecosystems where picophytoplankton dominates. For the subtropical gyre, we can assume that the rate of nutrient uptake is much faster than the vertical supply rate so that $\gamma \gg 1$. Two limits are of interest. The first, $\epsilon \gg 1$, corresponds to fast-sinking phytoplankton leading to a low-standing stock of biomass in the upper ocean:

$$p_{ss} \approx \epsilon^{-1} \tag{7}$$

The second, $\epsilon \ll 1$, corresponding to more slowly sinking small phytoplankton, leads to a large stock of biomass in the upper ocean:

$$p_{ss} \approx 1 - \epsilon \tag{8}$$

Both solutions are independent of the nutrient supply rate and illustrate that the system can achieve different levels of biomass regardless of the nutrient supply rate. Instead, the biomass level can depend on the efficiency with which nutrients are retained in the upper ocean. A low retention efficiency corresponding to particulate sinking rates that are fast compared to the supply rate ($\epsilon \gg 1$) leads to a low biomass $P \approx \frac{q}{s} N_d$. Conversely, a high retention efficiency corresponding to particulate sinking rates that are slow compared to the supply rate ($\epsilon \ll 1$) leads to a high biomass $P \approx N_d\left(1 - \frac{s}{q}\right)$.

Design of the ocean biogeochemical model. We wanted to test possible alternatives to nutrient supply that can result in an increase in biomass under

future climate conditions within a three-dimensional ocean circulation model. Our model reproduced the transport and cycling of three pools of *P*, dissolved inorganic *P* (DIP), DOP, and biomass (represented by the particulate fraction, POP). The *P* cycling component simulated the exchange of *P* among the three pools by the processes of production and remineralization of organic matter. We then did a sensitivity analysis to evaluate how changes in the remineralization and distribution of particles could affect phytoplankton biomass.

The circulation model reproduced global patterns of mass transport for each fraction (Supplementary Table 2). The circulation model was constrained using a data-assimilation technique that incorporated observations of several tracers[37,38]. The model simulated transport of the two dissolved forms (DIP and DOP) using an advection and diffusion operator **T** ($\mathbf{T} \equiv \nabla[U - k\nabla]$), which is an $N \times N$ sparse matrix (N: the number of wet grid boxes). **T** was constrained by multiple tracers including temperature, salinity, mean sea surface height, natural radiocarbon, CFC-11, air–sea heat exchange and freshwater sources[37,39]. Biomass is subject to sinking and remineralization as particulate organic matter in the water column following a power law function (that is, Martin curve). The exponential decay (b) was implicitly incorporated into a particle flux divergence operator (**F** in equation (10)) and was optimized as part of the inversion (Supplementary Table 2).

DIP losses were simulated as the phytoplankton uptake as well as transport, and DIP gains by remineralization and influx of deep water to the euphotic layer. DIP consumption rate was modelled using satellite-derived net primary production (NPP) together with two tunable parameters (α and β) (equation (9) and Supplementary Table 2)[39].

$$\gamma = \alpha \frac{[\mathrm{NPP}/R_{\mathrm{C/P}}]^{\beta}}{[\mathrm{DIP}]_{\mathrm{obs}}} \tag{9}$$

where the unit of NPP was converted to mmol m^{-2} s^{-1} of C, β is a dimensionless parameter and $R_{C/P}$ is the carbon-to-phosphate ratio. The assimilation rate (γ) had the same units as α (s^{-1}). Gains of DOP were simulated by DIP assimilation to organic matter and by POP dissolution, and losses were simulated by DOP remineralization. Gains of POP were simulated by DIP assimilation and losses by POP dissolution. Changes in the three components of the *P* cycle are summarized in equation (10).

$$\begin{aligned}
\left[\tfrac{d}{dt} + \mathbf{T}\right][\mathrm{DIP}] &= -\gamma[\mathrm{DIP}] + \kappa_{\mathrm{d}}[\mathrm{DOP}] + \kappa_{\mathrm{g}}\left([\mathrm{DIP}] - [\overline{\mathrm{DIP}}]_{\mathrm{obs}}\right) \\
\left[\tfrac{d}{dt} + \mathbf{T}\right][\mathrm{DOP}] &= \sigma\gamma[\mathrm{DIP}] + \kappa_{\mathrm{p}}[\mathrm{POP}] - \kappa_{\mathrm{d}}[\mathrm{DOP}] \\
\left[\tfrac{d}{dt} + \mathbf{F}\right][\mathrm{POP}] &= (1-\sigma)\gamma[\mathrm{DIP}] - \kappa_{\mathrm{p}}[\mathrm{POP}]
\end{aligned} \tag{10}$$

where $[\overline{\mathrm{DIP}}]$ is volume-weighted average DIP concentration; κ_g is a geological restore term, which is a small value (that is, $1/10^{-6}$ yr) and is used to restored DIP concentration to observed global mean; σ is a parameter that governed the partition of DIP assimilation in production of DOP and POP. We used $\sigma = 1/3$, which means that one-third of DIP is produced as DOP and the rest as POP (equation (10)). The term κ_d is the DOP remineralization rate optimized as part of the inversion (Supplementary Table 2). Finally, κ_p is the POP dissolution rate and is set at $\kappa_p = 1/30\ d^{-1}$.

Most ocean biogeochemical concepts and models include a direct or implied control of nutrient supply on upper ocean biomass. Thus, we used the model to explore three possible alternative mechanisms for regulation of upper ocean biomass and manipulated values within their known range. The first mechanism is based on the principle that increased temperature leads to smaller surface phytoplankton (such as *Prochlorococcus*) with lower sinking speed, leading to remineralization closer to the surface. To simulate this effect, we modified b in the range of ±15%. The second mechanism is that increased temperature leads to higher remineralization of DOP to DIP. To simulate this effect, we modified κ_d in the range of ±15%. The third mechanism is that the C/P ratio of phytoplankton is higher in a warmer, nutrient-deplete future ocean environment[28,40,41]. To simulate this effect, we compare biomass levels using C/P based on Redfield proportions (106/1) versus the empirical relationship determined by Galbraith and Martiny[40]. Finally, we tested the effect of a change with a combination of all mechanisms.

Data availability

All observations and phytoplankton model data are available at BCO-DMO (https://www.bco-dmo.org/project/764270). The biogeochemical model data are available here (https://zenodo.org/record/3543774).

Code availability

The biogeochemical model code is available at https://doi.org/10.5281/zenodo.3543779.

References

32. Morel, A. et al. Examining the consistency of products derived from various ocean color sensors in open ocean (Case 1) waters in the perspective of a multi-sensor approach. *Remote Sens. Environ.* **111**, 69–88 (2007).
33. Casey, J. R., Aucan, J. P., Goldberg, S. R. & Lomas, M. W. Changes in partitioning of carbon amongst photosynthetic pico- and nano-plankton groups in the Sargasso Sea in response to changes in the North Atlantic Oscillation. *Deep. Sea Res. Part 2 Top. Stud. Oceanogr.* **93**, 58–70 (2013).
34. Dunne, J. P. et al. GFDL's ESM2 global coupled climate–carbon Earth system models. Part II: carbon system formulation and baseline simulation characteristics. *J. Clim.* **26**, 2247–2267 (2013).
35. Taylor, K. E., Stouffer, R. J. & Meehl, G. A. An overview of CMIP5 and the experiment design. *Bull. Am. Meteorol. Soc.* **93**, 485–498 (2012).
36. Pearman, P. B., Guisan, A., Broennimann, O. & Randin, C. F. Niche dynamics in space and time. *Trends Ecol. Evol.* **23**, 149–158 (2008).
37. DeVries, T. & Primeau, F. Dynamically and observationally constrained estimates of water-mass distributions and ages in the global ocean. *J. Phys. Oceanogr.* **41**, 2381–2401 (2011).
38. Primeau, F. W., Holzer, M. & DeVries, T. Southern ocean nutrient trapping and the efficiency of the biological pump. *J. Geophys. Res. Ocean.* **118**, 2547–2564 (2013).
39. Teng, Y.-C., Primeau, F. W., Moore, J. K., Lomas, M. W. & Martiny, A. C. Global-scale variations of the ratios of carbon to phosphorus in exported marine organic matter. *Nat. Geosci.* **7**, 895–898 (2014).
40. Galbraith, E. D. & Martiny, A. C. A simple nutrient-dependence mechanism for predicting the stoichiometry of marine ecosystems. *Proc. Natl Acad. Sci. USA* **112**, 8199–8204 (2015).
41. Yvon-Durocher, G., Dossena, M., Trimmer, M., Woodward, G. & Allen, A. P. Temperature and the biogeography of algal stoichiometry. *Glob. Ecol. Biogeogr.* **24**, 562–570 (2015).

Acknowledgements

We thank the many contributing researchers for the oceanographic data and K. Mackey and J. Martiny at UCI for helpful comments. Financial support for this work was provided by the National Science Foundation (OCE-1046297 and OCE-1848576 to A.C.M.), CONICET, UBACYT (20020170100620BA), Agencia Nacional de Promoción Científica y Tecnológica (PICT-2017-3020 to P.F.) and US Department of Energy Office of Biological and Environmental Research (DE-SC0012550 to F.W.P.).

Author contributions

P.F. and A.C.M. designed the study, P.F., W.-L.W. and F.W.P. did the analysis and A.C.M. wrote the paper.

Competing interests

The authors declare no competing interests.

Additional information

Extended data is available for this paper at https://doi.org/10.1038/s41561-019-0524-2.

Supplementary information is available for this paper at https://doi.org/10.1038/s41561-019-0524-2.

Correspondence and requests for materials should be addressed to A.C.M.

Peer review information Primary handling editors: Xujia Jiang; Heike Langenberg.

Reprints and permissions information is available at www.nature.com/reprints.

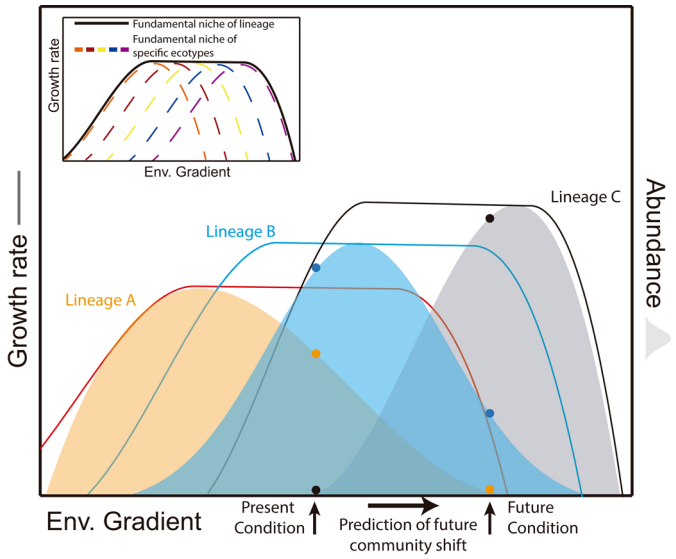

Extended Data Fig. 1 | Conceptual model for linking ecotype diversity, environmental, and biotic factors to the fundamental and realized niches of phytoplankton lineages.

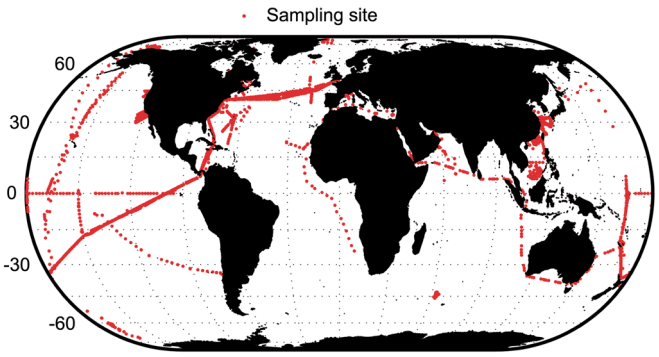

Extended Data Fig. 2 | Global distribution of sampling sites for the 13,771 observations used in this study.

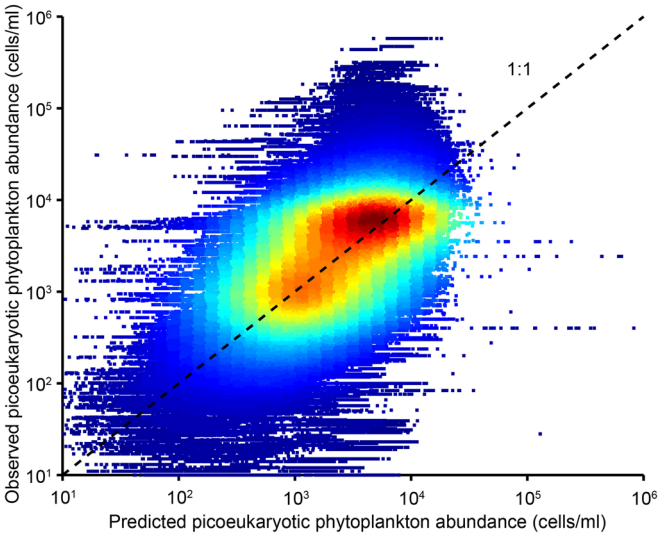

Extended Data Fig. 3 | Scatter density for observed versus predicted picoeukaryotic phytoplankton cell abundance. Cell abundances were predicted based on ancillary environmental information associated with each observation. The dashed line represents the 1:1 relationship.

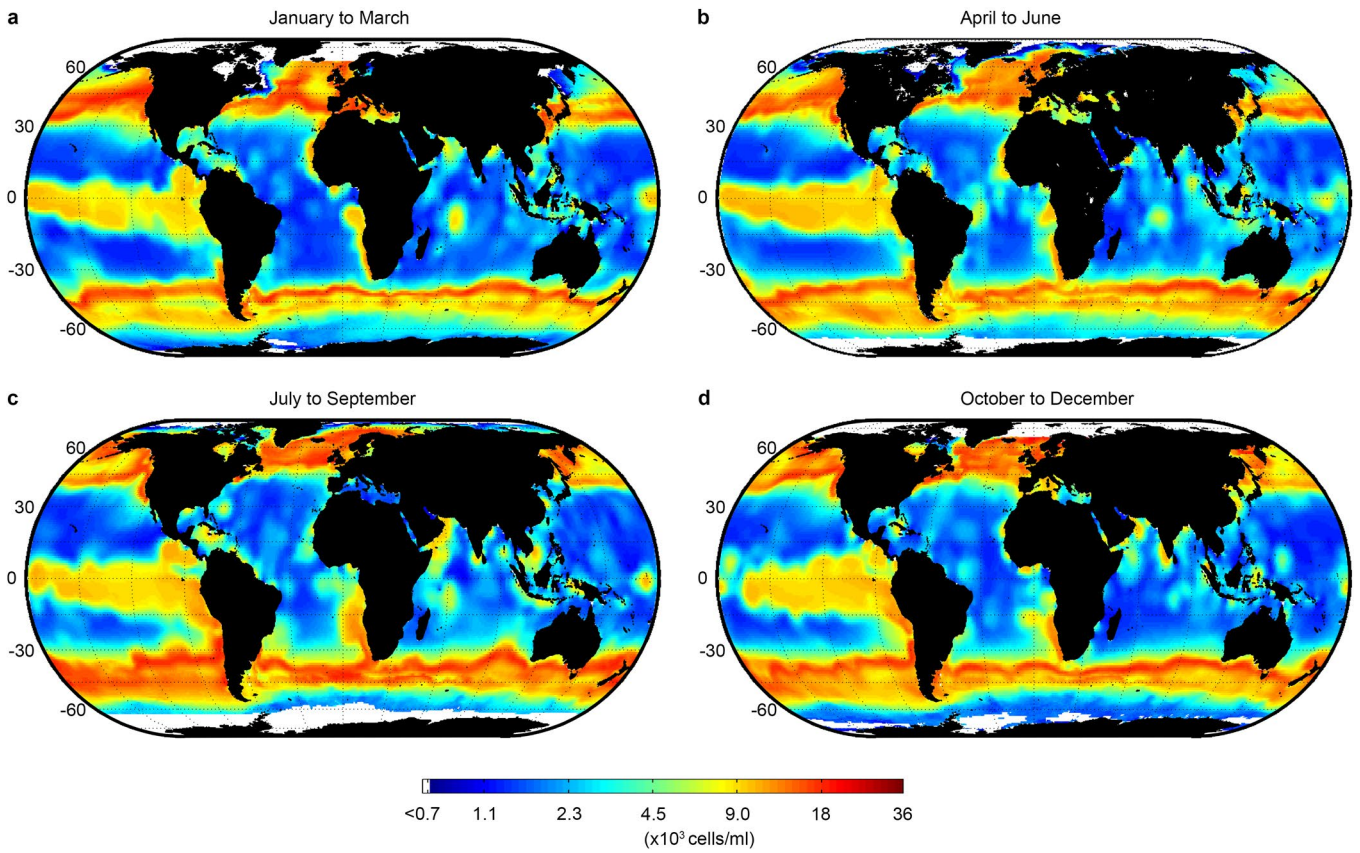

Extended Data Fig. 4 | Predicted seasonal distributions of picoeukaryotic phytoplankton at the surface. Mean quarterly surface picoeukaryotic phytoplankton abundance for (a) January to March, (b) April to June, (c) July to September, and (d) October to December.

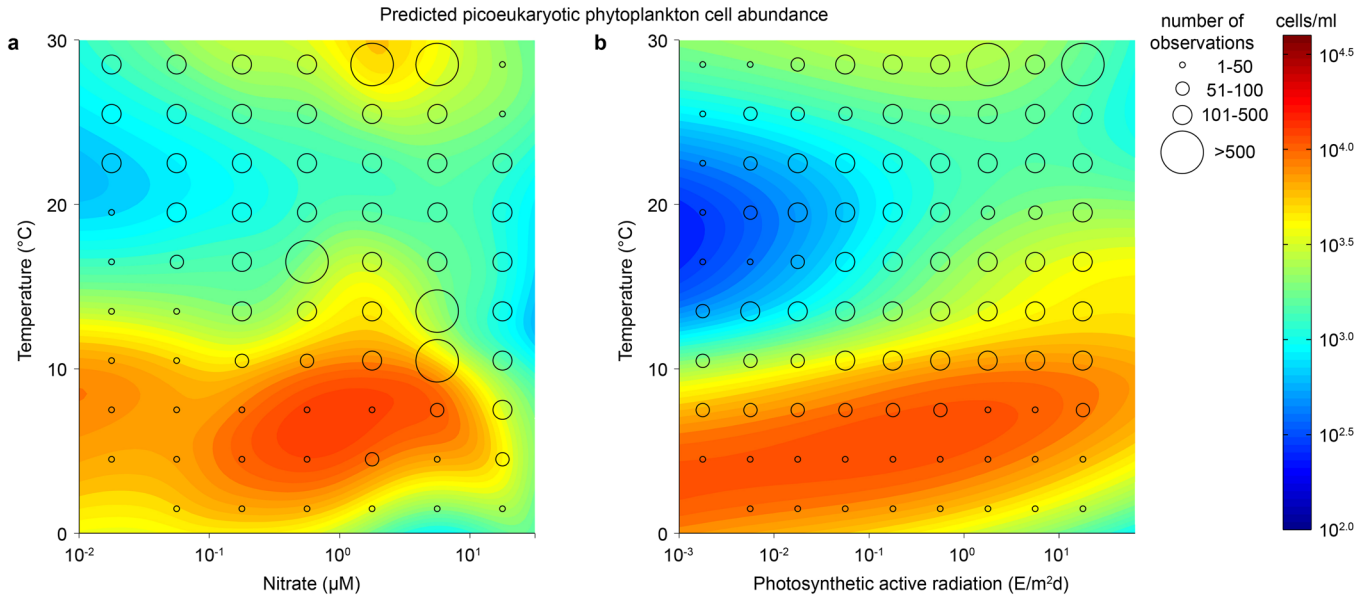

Extended Data Fig. 5 | Predicted picoeukaryotic phytoplankton cell abundance and number of observations for the combination of temperature and (a) nitrate, and (b) photosynthetic active radiation (PAR). The predicted abundance represents the mean quantitative niche model output based on 100 trained neural networks at constant (a) PAR (3.2 E m^{-2} d^{-1}) and (b) nitrate (3.2 μM). Circle size represents the number of observations on a gridded combination of environmental variables.

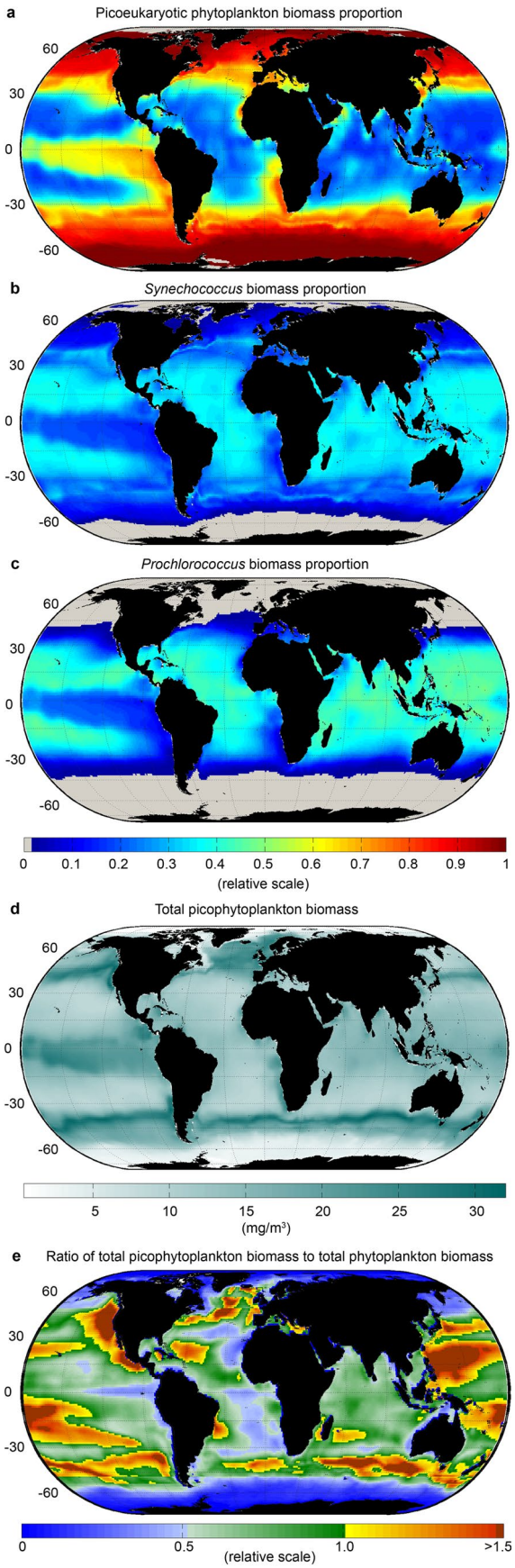

Extended Data Fig. 6 | See next page for caption.

Extended Data Fig. 6 | Distribution of total picophytoplankton carbon biomass and relative contribution of each lineage at the ocean surface. Proportional contribution to total picophytoplankton carbon biomass by (a) picoeukaryotic phytoplankton, (b) *Synechococcus* and (c) *Prochlorococcus*. (d) Total picophytoplankton carbon biomass. (e) Proportional contribution of picophytoplankton to total phytoplankton carbon biomass. Total picophytoplankton carbon biomass was estimated as the sum of picoeukaryotes, *Synechococcus* and *Prochlorococcus* cellular abundance weighted by their cellular carbon biomass. Total phytoplankton biomass was predicted by the GFDL ES2M model.

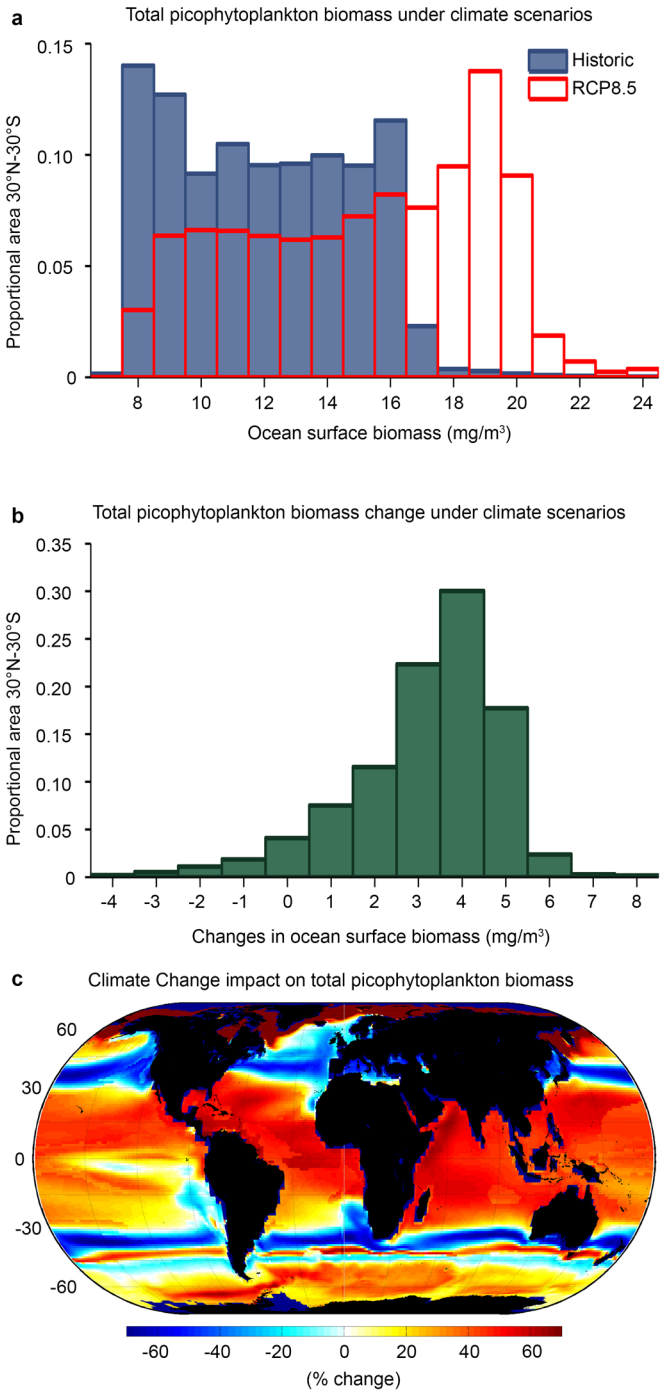

Extended Data Fig. 7 | Projected impact of climate change on total picophytoplankton carbon biomass. Proportional area in the 30˚N-30˚S band accounted for by (a) total picophytoplankton biomass concentration for the historic and RCP8.5 CMIP5 scenarios, and (b) changes in biomass between RCP8.5 and historic CMIP5. (c) Percentage of change in surface total picophytoplankton carbon biomass estimated for the end of 21st and 20th centuries based on temperature and nitrate concentration simulated under the RCP8.5 and historic CMIP5 scenarios.

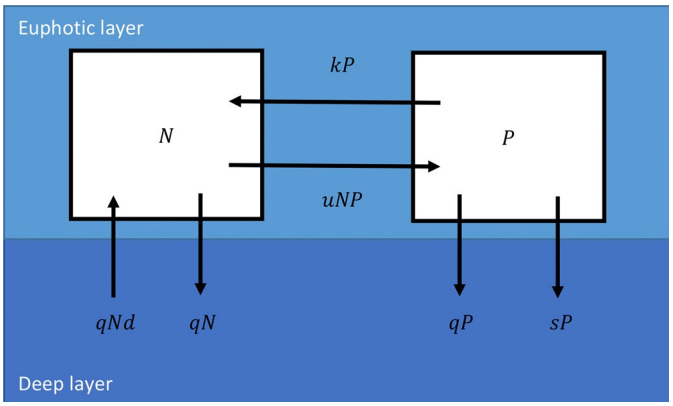

Extended Data Fig. 8 | Design of a simple model describing the relationship between nutrient cycling and standing stock of phytoplankton biomass. Fluxes are identified by arrows and stocks by boxes. *N* and N_d represent nutrient concentration at the euphotic and deep layer respectively, and *P* represents phytoplankton biomass. *k* represents phytoplankton remineralization rate, *u* the phytoplankton nutrient uptake rate, *s* the phytoplankton sinking rate, and *q* the vertical mixing rate.

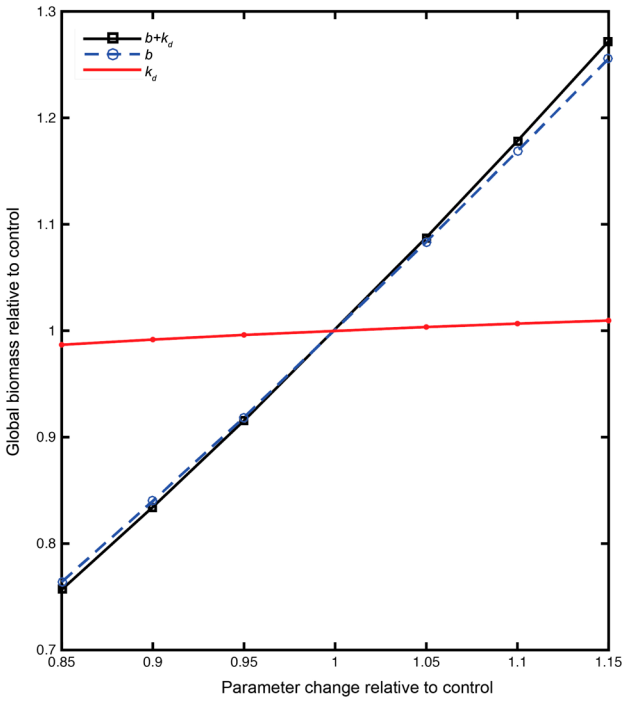

Extended Data Fig. 9 | Sensitivity of global picophytoplankton biomass to changes in remineralization rates estimated with an ocean biogeochemical model. *b* is the exponential decay of particulate organic matter in the water column following a power law Martin curve that represents nutrient trapping, and κ_d is the remineralization rate of DOP to DIP. Global biomass for the control used values in Table S2.

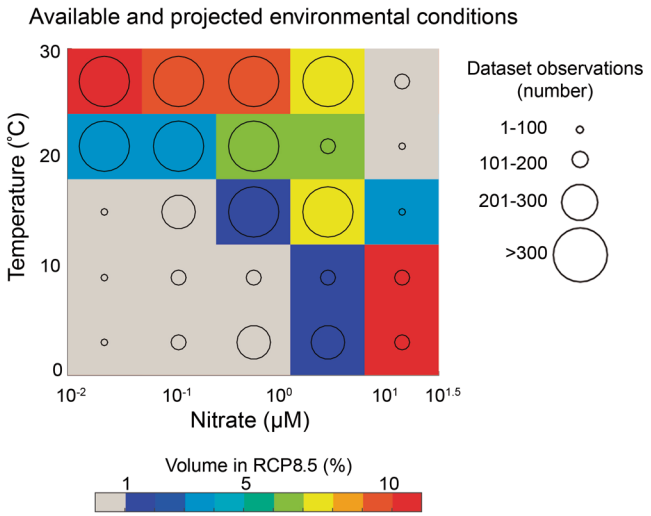

Extended Data Fig. 10 | Availability of observations to inform future environmental conditions. Number of observations and percent of ocean volume for the RCP8.5 in a combination of temperature and nitrate.